Development of a Stereo Camera System for Monitoring Hydrokinetic Turbines

James Joslin, Brian Polagye, and Sandra Parker-Stetter
Northwest National Marine Renewable Energy Center
University of Washington
Seattle, WA 98115
email: jbjoslin@u.washington.edu

***Abstract*—The implementation of a hybrid optical-acoustic imaging system is described and evaluated for environmental monitoring of a hydrokinetic turbine. This monitoring system is intended to provide real time stereographic imagery in the near field ($\geq$10 m) of tidal turbines proposed for deployment in Admiralty Inlet, Puget Sound, Washington. Post deployment observations will provide valuable information about the frequency and character of interactions of marine animals with the turbine. Optical camera effectiveness is evaluated under realistic field conditions in order to determine the range within which it is able to detect, discriminate, and classify targets. These field evaluations serve to inform optimal system placement relative to the turbine. Preliminary assessment of image quality and measurements taken by the stereographic cameras show that it will likely be able to discriminate and classify targets at ranges up to 3.5 m and detect targets at ranges up to and potentially beyond 4.5 m.**

***Index Terms*—Environmental Monitoring, Stereo Imagery, Hydrokinetics, Tidal Turbines**

I. Introduction

The energy in fast moving tidal currents is a potential source of renewable, predictable electricity. Single-turbine demonstration projects have successfully deployed with rated capacities exceeding 1 MW [1]. Tidal turbines harness tidal currents in a manner analogous to wind turbines and this emerging industry has benefited from the lessons learned in the development of wind energy. However, before large-scale utilization of tidal current resources may occur, the approach must be proven to be not just technically feasible, but economically viable, environmentally compatible, and socially acceptable.

Potential environmental impacts have been identified by, among others, Cada et al. [2] and Polagye et al. [1]. However, the frequency with which the most significant impacts will actually occur is uncertain (e.g., direct mortality or increased predation of an endangered species). Resource agencies have expressed particular interest in understanding the type and frequency of close-range interactions between marine animals (fish, large invertebrates, marine mammals, and diving seabirds) and tidal turbines. Possible interactions include collision/strike with the moving rotor, attraction due to artificial reef effects, and avoidance due to pressure fluctuations or sound. To date, there have been several attempts to collect this information with active acoustics (e.g., sonars or echosounders). These have provided valuable information about the behavior of fish in the vicinity of turbines (e.g., [3]), but have found it difficult to achieve a fine level of taxonomic classification or characterize the nature of interactions with the turbine rotor itself.

Snohomish Public Utility District has proposed to deploy two turbines manufactured by OpenHydro, Ltd (www.openhydro.com) in northern Admiralty Inlet, Puget Sound, Washington [4]. The turbines are horizontal axis devices 6 m in diameter and would operate for a five year period as a demonstration project to evaluate environmental effects and turbine reliability. If the demonstration project is successful, Admiralty Inlet has significant potential for large-scale tidal energy utilization [5]. The water depth in the project area is approximately 55 m and the turbine hub height is 10 m above the seabed. During strong tidal exchanges, currents exceed 3 m/s [6]. Environmental studies proposed for this project include characterizing direct interaction between marine animals and the turbine rotors. The imaging system described here has been developed to implement those studies.

II. Methodology

A. Imaging System Description

The objectives for implementation of the imaging system for turbine monitoring are to classify targets (e.g., taxonomic classification to the species level, if possible) within the near-field environment (e.g., up to 10 meter range) of an operating hydrokinetic turbine. The relative velocity between the camera and these targets will be on the order of several meters per second. Shore power and fiber optic data connectivity will be available. The imaging system will need to operate for multi-month periods between planned maintenance cycles. Engineering constraints are overall cost, complexity, and data bandwidth.

The imaging system developed in response to these objectives is a hybrid optical-acoustic system, incorporating stereographic optical cameras and a high-resolution multibeam sonar (acoustic camera). As described in Sec. 2.2, calibrated stereo cameras can provide information about the absolute position, size, and speed of targets. Target size is particularly relevant to classifying targets.

The depth to which the camera system is to be deployed (approximate hub height of turbine) is expected to have minimal ambient light. Water quality surveys indicate low turbidity ($<$1 NTU), but biological flocculent limits the effective range

of lighted video [7]. The lack of ambient light necessitates artificial lighting. Further, in order to capture crisp images with relative motion on the order of 3 m/s, an exposure time between 2 and 50 μs is recommended [8]. This can be achieved by strobe illumination. Increased camera-light separation improves the effective range by reducing backscattered light from turbidity and flocculent [9]. However, the camera-light separation is constrained by the need to periodically recover the system to the surface for maintenance.

The use of full-spectrum, artificial light has the potential for behavioral effects on fish and invertebrate species (attraction or avoidance). It is intended that the acoustic camera be used to characterize the effect of strobe illumination and determine a minimum cool down time between exposure to strobe illumination and resumption of pre-illumination behavior. For this reason, an acoustic camera with a field of view similar to the optical cameras is preferred.

The principle components of the imaging system are, therefore, a pair of cameras, strobe illuminators, acoustic camera, and the power/communications architecture to integrate them and communicate with shore via the fiber optic link. To minimize system cost and complexity, the primary communications bus operates on Ethernet protocol, with media conversion from copper to fiber to extend its range. A secondary communications bus operates on RS-232 protocol (RS-232 communications converted to Ethernet) and is used to monitor the health of various components (current draw, temperature, and humidity) and control power distribution. Media conversion limits the total bandwidth to 1 Gb/s (125 MB/s).

The primary trade-offs in camera selection are resolution, bandwidth, and cost. High resolution increases the potential for target classification, but at high frame rates (e.g., 10 Hz) data bandwidths can easily exceed the capacity of the communications system. The selected cameras are Allied Vision Technologies Manta G-201 B/Cs (2 Megapixel). These are compact, industrial-grade machine vision cameras operating on Gigabit Ethernet (GigE) vision protocols (www.alliedvisiontec.com). The cameras are equipped with 5 mm focal length lenses (Navitar NMV-5M23). A wider field of view could be achieved with a shorter focal length lens, but at the cost of image resolution. For strobe illumination, four Excelitas Technologies MVS-5000 units were selected on the basis of their performance in underwater camera systems with similar specifications [10]. A BlueView P900/2250 (www.blueview.com) was selected as an acoustic camera due to a similar field of view to the optical cameras, as well as its Ethernet-based communications bus.

With the exception of the BlueView acoustic camera, the system components are not designed for underwater use and must be enclosed within pressure housings. The pressure housings for the optical cameras and strobes are anodized aluminum with double seal O-rings on the end caps and acrylic optical view ports (planar). As shown in Fig. 1, these modular components are mounted to an aluminum frame, resulting in nearly overlapping fields of view between the optical and acoustic cameras and a camera-strobe separation distance of

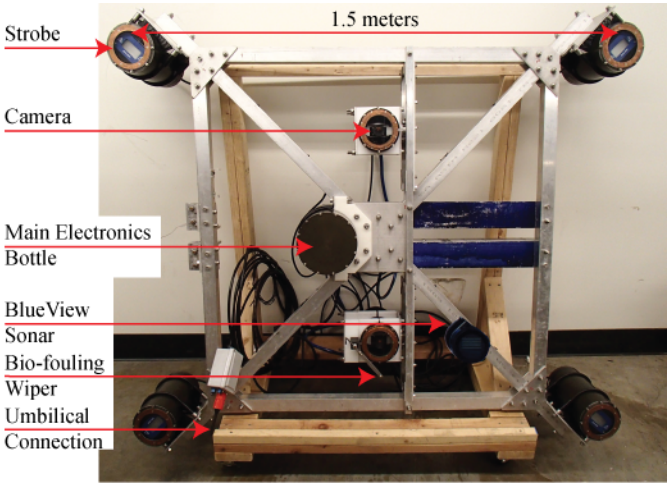

Fig. 1: Prototype imaging system showing principal components and scale

1 m. Optical camera separation is adjustable between 0.5 and 1.1 m.

Without mitigation measures, biofouling of the optical ports will rapidly degrade system effectiveness. To address this, a mechanical wiper (Zebra-Tech Hydro-wiper, www.zebra-tech.co.nz) was integrated into each housing and copper rings placed around the perimeter of the optical ports.

Off-the-shelf component specifications and costs are detailed in Table I. Power requirements for system components are described in Table II. Custom electronics were developed to step down main supply power (400 VDC) to 12 V component supply. Medium voltage DC power supply is required to minimize resistive losses over the long cable run between the turbine and shore station. Temperature, humidity, and current monitoring in individual bottles also utilizes custom electronics. The strobes are, unsurprisingly, the highest power draw in the system.

System operation, monitoring, camera control, and optical image acquisition are performed with the National Instruments LabView serial communications VISA and image acquisition IMAQ modules (www.ni.com/labview). The image acquisition module is configured to allow users to directly control a limited subset of camera settings, such frame rate, exposure time, gain, strobe operation, and strobe delay. Simultaneous image acquisition from both cameras is achieved by the virtual shutter effect due to the short strobe duration (20 μs) in the absence of ambient light. The acoustic camera requires a proprietary software package (ProViewer).

B. Laboratory Evaluation

Stereographic imagery uses two cameras to map three-dimensional space from two-dimensional images. Their relative separation and orientation and fields of view must be fixed. Given information about the relative geometry of the two cameras, the position of targets that fall within the field of view of both cameras may be determined through stereo-

TABLE I: Component, manufacturer, description, and equipment cost for the stereo-camera portion of the turbine monitoring instrumentation.

Component	Manufacturer	Description	Unit Cost
Optical Cameras	Allied Vision Technologies, Manta G-2-1B/C	2 Megapixel, GigE Vision Camera with Sony ICX274 Sensor, 1624x1234 pixels, 4.4 μm pixel cell size, 1/1.8" sensor size, 14 fps.	$1600
Lenses	Navitar NMV-5M23	2/3" Megapixel format with manual focus from 0.05 m to infinity and 2.8 to 16 F-stop.	$500
Strobes	Excelitas Technologies MVS-5000	20 μs flash duration, 30 Hz maximum flash rate.	$1300
Acoustic Camera	BlueView P900/2250	Dual frequency sonar with 45°x 20°field of view, 60 m (900 kHz) and 8 m (2.25 MHz) maximum range.	$30,000
Mechanical Wipers	Zebra-Tech LTD	Brush style hydro fouling optical port wiper.	$1200

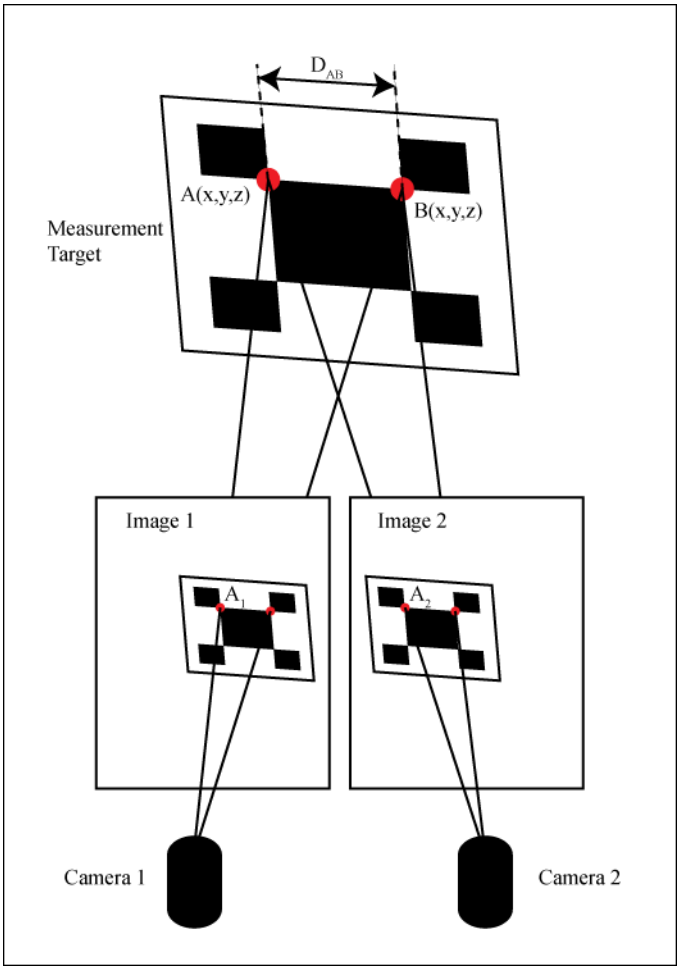

Fig. 2: Stereo-triangulation and distance measurement (after [11])

TABLE II: Component power requirements at maximum data acquisition rates.

Component	Mode	Power Requirement
Optical Cameras (2)	Acquiring at 10 fps	10 W
Strobes (4)	Strobing at 10 Hz	72 W
Mechanical Wipers (6)	3 wiper motors locked (high failure rate)	18 W
Acoustic Camera	Acquiring	19 W
Media conversion and auxiliary loads	Operating	30 W
Transformer Losses	80% efficient	37 W
Total System		**186 W**

triangulation. Triangulation uses the horizontal and vertical pixel coordinates (x, y) of a point in each image (A_1 and A_2) to determine the three-dimensional coordinates of that point in space A(x,y,z). The point locations in the two dimensional images are related by

$$A_1 = RA_2 + T \tag{1}$$

where R is the rotation matrix and T is the translation vector relating camera 1 to camera 2. Size measurements are made from the stereo images by computing the Euclidean norm between two triangulated points (A and B) in the same image pairs, as shown in Fig. 2. Selection of the same target point in both images is essential for accurate triangulation. The velocity of objects may be calculated from the distance a single point moves over sequential frames of imagery.

The field of view of the individual cameras was measured by acquiring images of a graduated rule, that spanned the horizontal axis of the image, mounted at a known distance from the camera. These images were captured with the camera underwater to account for barrel distortion on the lens and refraction at the air/water interface associated with the camera lens and optical port on the pressure housing. The overlapping field of view of the stereo system depends on the camera offset distance and toe-in angle, which may be optimized for observations at a given distance.

The calibration procedure for the stereo camera system closely follows the methods described in Williams et al. [11].

Images of a one-meter square calibration target with a 7 x 8 checkerboard pattern of 10 cm squares were collected in an indoor, saltwater pool from both cameras at distances of 3 to 6 meters. With the camera system suspended approximately one meter below the surface of the water, the target was moved through the water while images were collected to obtain a variation in target angles throughout the field of view of both cameras. Forty-five image pairs that represented a good distribution of the target orientations and separation in the area of interest were then analyzed with the freely available camera calibration toolbox for Matlab [12].

The Matlab software uses the Harris corner finding algorithm based on color gradients to locate the square corners on the calibration target in each image [13] and estimates the intrinsic parameters of the individual cameras based on user provided information about the actual target size. These parameters include the focal length, principal point, skew, and distortion coefficients, which account for all barrel distortion of the images and may be used to rectify images taken with the camera. With the estimated intrinsic parameters for the individual cameras, stereo calibration is used to estimate the extrinsic parameters of the camera system by analyzing the target position in the image pairs and iteratively computing the epipolar geometry [14]. This process provides estimates for the rotation and translation vectors of the right camera with respect to the left camera, which may be used for triangulation.

Along with the best estimates for the intrinsic and extrinsic parameters of the camera system, the calibration procedure also provides the standard deviation of pixel error for each camera. These errors are the measured distance between the corners found using the Harris method during calibration and the expected corner location based on a reprojection of the target on each image processed. Careful navigation of the calibration procedure is necessary to minimize pixel error.

C. Field Evaluation

One of the key uncertainties regarding the integration of the imaging system with a tidal turbine is the functional range for detection, discrimination, and classification of marine animals by the stereographic cameras. The functional range establishes where the imaging system should be deployed relative to the turbine rotor. A secondary question is the relative effectiveness of acoustic and optical camera systems. The main variables that could affect imaging system effectiveness to classify a target are: the target range, relative velocity of the target, attenuation of artificial lighting by flocculent, and the cameras′ digital gain.

Given the difficulty of accurately simulating flocculent and high relative velocities between targets and the camera in a laboratory setting, a field evaluation was undertaken. For this purpose, the imaging frame shown in Fig. 3 was fabricated. The frame consisted of a hard point mount for the imaging system located 4.5 m above the base of the frame. It is lead-ballasted and has in-air weight approaching 3000 lbs. Relative water velocities of up to 2 m/s were achieved by towing the imaging frame by a high-tensile strength umbilical cable

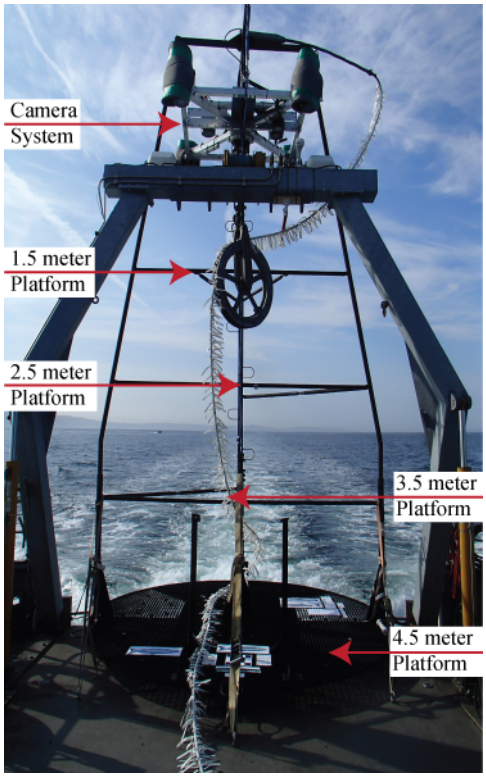

Fig. 3: Imaging frame for camera testing.

with power and fiber optic connections. Various targets were attached to platforms at camera-target separation distances of 1.5 m, 2.5 m, 3.5 m, and 4.5 m. Targets included static objects, such as a version of the calibration image described in Sec. 2.2, standard eye charts, and line drawings of fish. The latter included large adult salmon (42 cm fork length), as well as small juvenile salmon and Pacific herring (5-11 cm fork length). Fish drawings were on a white or green background to provide either low or high contrast respectively. In addition, tape streamers were attached to the frame and used to evaluate the ability of the camera system to freeze rapid, complex motions.

In addition to image acquisition by the optical and acoustic cameras, several types of ancillary data were collected to interpret results. Cosine irradiance light meters (HOBO Pendant Temp-Light, www.onsetcomp.com) were attached to the camera frame and imaging frame platforms. These were intended to characterize the intensity of strobe illumination, but their response time was insufficiently slow to achieve this, even at 10 Hz strobe rates and 1 Hz sampling rate. However, as discussed below, information from the light meters was used to characterize the light attenuation coefficient tests and evaluate ambient light levels. Pressure loggers (HOBO U20 Water Level, www.onsetcomp.com) were attached to the camera frame and the base of the imaging frame to monitor depth at a sampling rate of 1 Hz. During tows, the umbilical wire angle was significant, up to 40^{o} at maximum tow velocities. Vibration was monitored by accelerometers on each platform and on

the camera frame (HOBO Pendant G, www.onsetcomp.com) logging at 1 Hz. Relative water velocity was monitored by a through-hull mounted Doppler profiler (RDI Workhorse 300 kHz, www.rdinstruments.com). Single Doppler profiler data was recorded and ensemble averaged over the duration of image acquisition. Water depth was monitored by the tow vessels echosounder and location monitored by differential GPS, both logged at 1 Hz in Nobeltec (www.nobeltec.com).

Co-temporal profiles of depth and illumination obtained while the imaging frame was being lowered for testing were used to evaluate the attenuation coefficient by fitting them to a profile of the form

$$I(z) = I_o e^{-cz} \tag{2}$$

where I is illumination (Lux), z is depth (m), and c is the empirical attenuation coefficient.

Qualitative assessments of imaging system performance included observations of flocculent and clarity of both the eye charts and fish line drawings. A quantitative assessment of performance was obtained by calculating the size of the black square on the calibration target from image pairs under different test conditions using the techniques described in Sec. 2.2. Absolute measurement error for each image pair was defined as

$$e = L_{measured} - L_{actual} \tag{3}$$

where $L_{measured}$ and L_{actual} are the stereographically measured and actual length of the calibration square, respectively. For ease of presentation, e is quantified in units of mm.

Tow tests were undertaken August 13-16, 2012 in northern Admiralty Inlet, Puget Sound, Washington. All tows were conducted by the University of Washington Applied Physics Laboratorys research vessel, the *R/V Jack Robertson*. Testing occurred during periods of falling tidal currents on greater ebb and flood to characterize performance during periods when biological flocculent would be stirred up by intense tidal currents. During each tow, targets were positioned on the imaging frame at a camera-target separation distance of either 2.5 m, 3.5 m, or 4.5 m. Preliminary testing undertaken in April, 2012 indicated shading of lower platforms by upper platforms could significantly degrade image quality when multiple platforms were simultaneously employed. These tests also indicated that targets were easily classified at 1.5 m range. Consequently, each test involved targets at a single separation distance and no tests were undertaken at separation distances smaller than 2.5 m. During each test, the imaging frame was lowered until the bottom of the frame (4.5 m distance from the cameras) was at a depth of 50 m. Images were acquired in blocks of fifty pairs at frame rates of 5-10 fps under the following conditions:

- Camera-target separation: 2.5 m, 3.5 m, 4.5 m
- Relative water velocity: near-zero (free-drift), $\sim$ 2 m/s (tow)
- Optical camera gain: $0x$, $10x$, $20x$

TABLE III: Calibration reprojection error values for each camera.

	Camera 1	**Camera 2**
Horizontal and vertical pixel error (x,y)	0.0548, 0.06011	0.1022, 0.1142
Localization uncertainty at 3.5 meters (x,y) [mm]	0.115, 0.130	0.215, 0.248

Each set of tests also included optical image capture with the strobes off and a gain of $20x$, to evaluate the capabilities of the optical cameras without artificial illumination. Absolute measurement error (e) was evaluated for thirty image pairs under each of the test conditions using Eq. 3.

III. Results

A. Laboratory Performance

The measured field of view of the individual cameras is approximately 54^o and 42^o in the horizontal and vertical directions (x and y), respectively. At a distance of 3.5 meters, this corresponds to a pixel size of 2.10 mm by 2.17 mm and an overall field of view of 3.4 m by 2.7 m.

As described in Sec. 2.2, uncertainty in stereographic localization is quantified as pixel error, as detailed in Table III. The pixel error associated with each cameras calibration represents a standard deviation for position error of approximately 0.2 mm for targets at a distance of 3.5 m (measured perpendicular to the center of the camera pair). This position error varies throughout the stereographic field of view, but manifests as a position bias for fixed points in space. Estimated error values for Camera 2 are approximately twice that of Camera 1. This is likely due to fogging on the optical port that was not noted until during the field deployment.

Original and rectified images from each camera are shown in Fig. 4 with the barrel distortion effects clearly visible in the curvature of the windows along the edges of the original images, but absent in the rectified images.

B. Field Performance

Four co-temporal depth/light profiles are evaluated to characterize ambient light at testing depth using the procedure described in Sec. 2.3. These were collected on August 13-16th. Values for the attenuation coefficient (c) ranged from 0.15 to 0.24 m^{-1}, which is within the range of values expected for coastal waters [9] and confirms earlier measures of site-specific turbidity. Attenuation in embayments can be an order of magnitude higher [15], which would significantly degrade the performance of the optical cameras.. Preliminary review of optical camera imagery indicates that artificial lighting is required below a depth of approximately 30 m to detect targets. This corresponds to an estimated ambient light level of 5 Lux. This is approximate from the calculated attenuation coefficient, since the noise floor for the light meters used in this study was 10 Lux (illumination less than 10 Lux logged as zero).

Table IV details the conditions tested, in terms of the experimental variables and site conditions. Specifically, z is

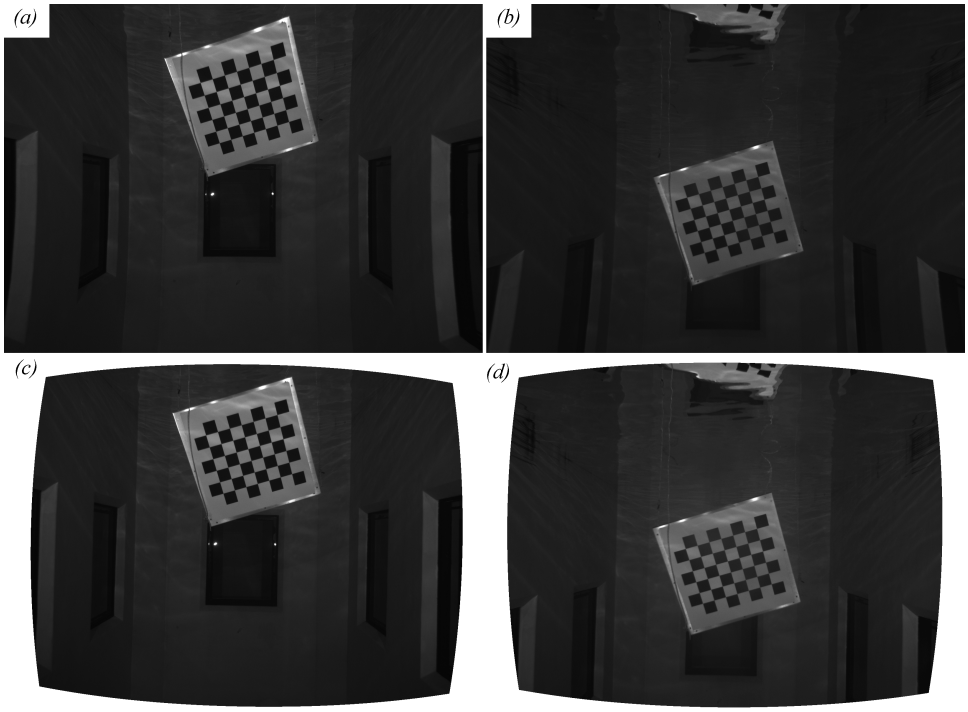

Fig. 4: Camera 1 and Camera 2 calibration images before (a and b, respectively) and after (c and d, respectively) after rectification. Effects of barrel distortion are visible in the curvature of the windows.

TABLE IV: Camera evaluation cases from tow testing.

		Digital Gain		
Camera-Target Separation	**Relative Velocity**	None (G = 0x)	G = 10x	G = 20x
2.5 m	0 m/s	z = 46 m, H = 61 m, u = 0.2 m/s	z = 46 m, H = 61 m, u = 0.7 m/s	z = 46 m, H = 61 m, u = 0.2 m/s
	2 m/s	z = 30 m, H = 70 m, u = 1.9 m/s	z = 33 m, H = 70 m, u = 2.0 m/s	z = 31 m, H = 69 m, u = 1.8 m/s
3.5 m	0 m/s	$NotTested$	$NotTested$	z = 51 m, H = 60 m, u = 0.3 m/s
	2 m/s	z = 36 m, H = 56 m, u = 2.1 m/s	z = 37 m, H = 56 m, u = 1.7 m/s	z = 36 m, H = 57 m, u = 1.8 m/s
4.5 m	0 m/s^a	z = 46 m, H = 60 m, u = 0.3 m/s	z = 46 m, H = 60 m, u = 0.2 m/s	z = 46 m, H = 61 m, u = 0.2 m/s
	2 m/s^b	z = 30 m, H = 66 m, u = 2.1 m/s	z = 30 m, H = 66 m, u = 1.9 m/s	z = 30 m, H = 66 m, u = 1.9 m/s

[a] Pressure logger data unavailable. Camera depth estimated from umbilical length.
[b] Pressure logger data unavailable. Camera depth estimated from umbilical length and wire angle for other comparable platform tests and level of ambient light (zero reading on light meters).

the depth of the camera frame, H is the total water depth, and u is the relative velocity between the imaging frame and the water. Of the desired test matrix only two gain settings were not evaluated, both for the 3.5 m platform.

Qualitatively, the optical imaging system performed well, as shown in Fig. 5. As expected, image clarity degrades with distance (Fig. 6) due to a combination of light attenuation, backscatter, and increasing pixel size. Strobe illumination is effective at freezing motion, with the streamers captured crisply in the frame (e.g., 3.5 m separate, 20x gain). At most camera-target separations, some degree of digital gain is required to detect the targets, though the high gain setting obscures image details at close separation distance (e.g., 2.5 m, 20x gain). Flocculent is apparent in video sequences, but the camera-strobe separation is largely effective at suppressing backscatter observed in ROV surveys in the project area (i.e., flocculent in ROV surveys appears much as snow in headlights and greatly restricts functional range). There are no distinguishing differences between images captured under tow, with a high flocculent flux, and those captured free drifting, with a low flocculent flux (not shown).

The acoustic camera was capable of imaging the test frame and detecting streamer motion, but the two-dimensional images could not be (obviously) used to detect the static targets on the frame, as shown in Fig. 7 for co-temporal images obtained by the two types of cameras.

Figure 8 shows absolute measurement errors (e) in the length of the calibration target square for each combination of gain setting and camera-target separation for the optical camera. At 2.5 m and 3.5 m camera-target separation there is a slight negative bias (length contraction) on the order of 2 mm and uncertainties are similarly small. Bias may be

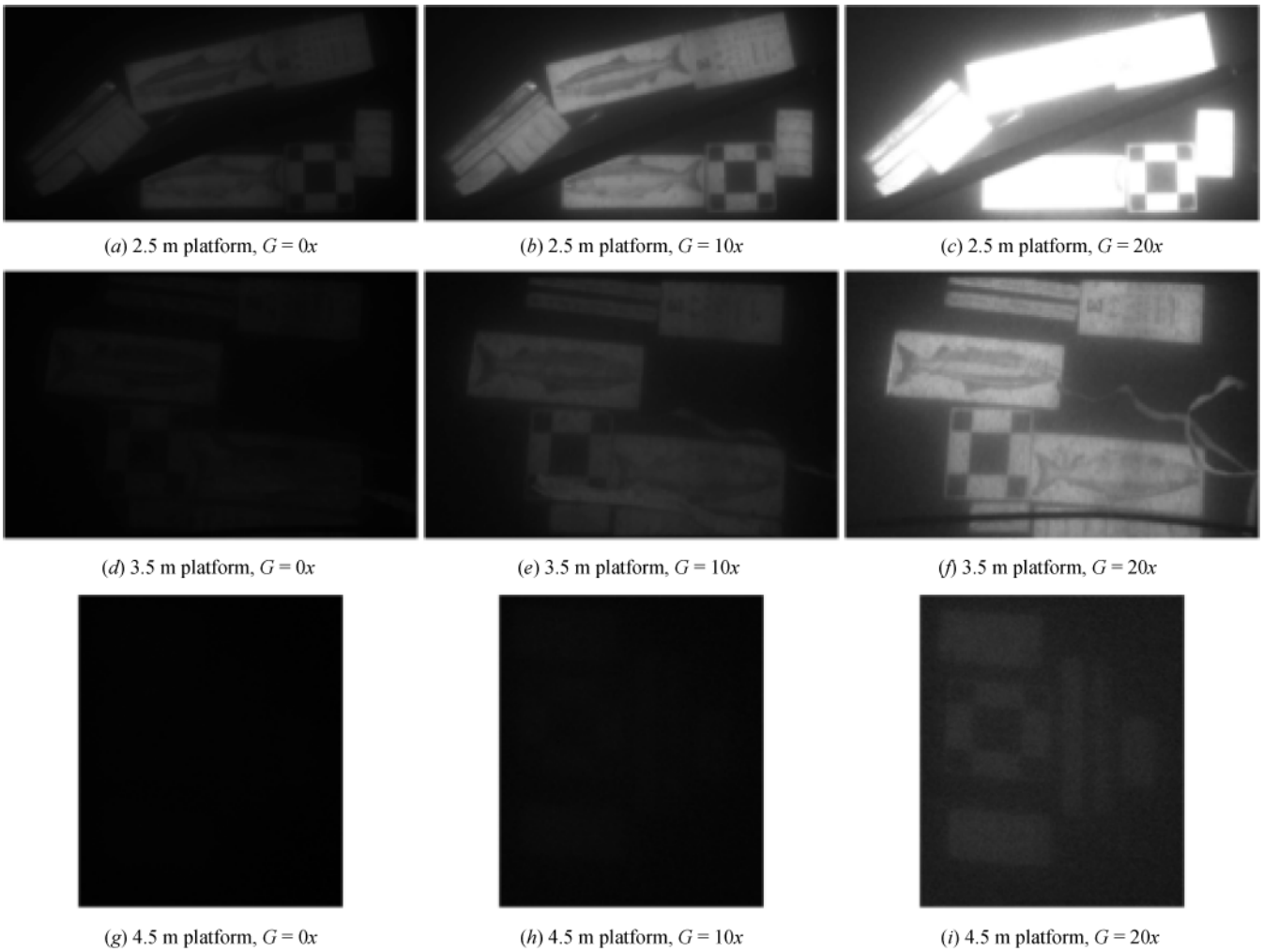

(*a*) 2.5 m platform, $G = 0x$ (*b*) 2.5 m platform, $G = 10x$ (*c*) 2.5 m platform, $G = 20x$

(*d*) 3.5 m platform, $G = 0x$ (*e*) 3.5 m platform, $G = 10x$ (*f*) 3.5 m platform, $G = 20x$

(*g*) 4.5 m platform, $G = 0x$ (*h*) 4.5 m platform, $G = 10x$ (*i*) 4.5 m platform, $G = 20x$

Fig. 5: Images acquired during testing under tow ($u \approx 2$ m/s) (image h detectable at full resolution on a large screen).

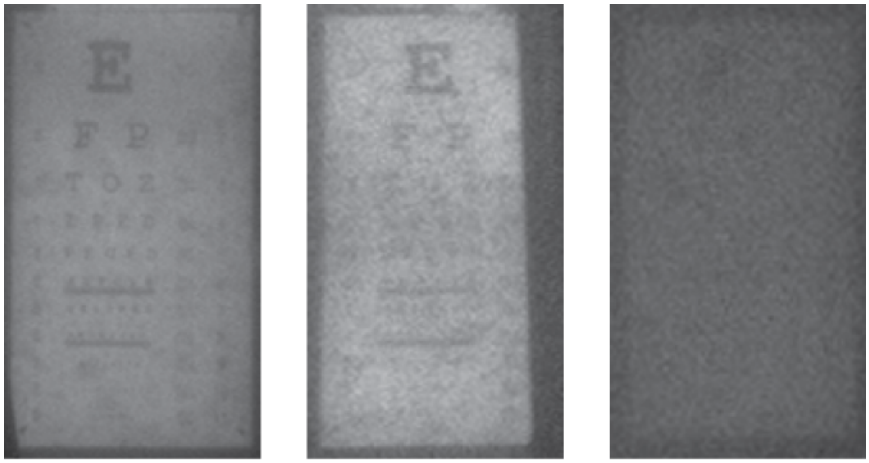

(*a*) 2.5 m platform, $G = 10x$ (*b*) 3.5 m platform, $G = 20x$ (*c*) 4.5 m platform, $G = 20x$

Fig. 6: Detail of eye charts (same base images as Fig. 5).

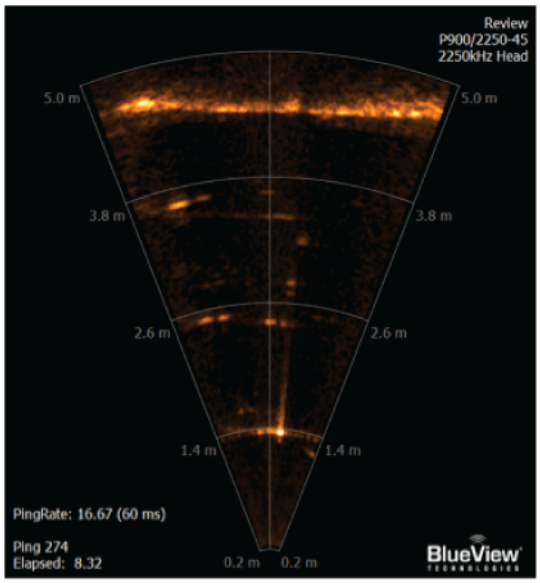

(*a*) Acoustic camera – acoustic returns at 1 m spacing correspond to the imaging frame platforms.

(*a*) Optical camera: camera-target separation = 4.5m, G = 20x

Fig. 7: Simultaneous optical and acoustic camera images.

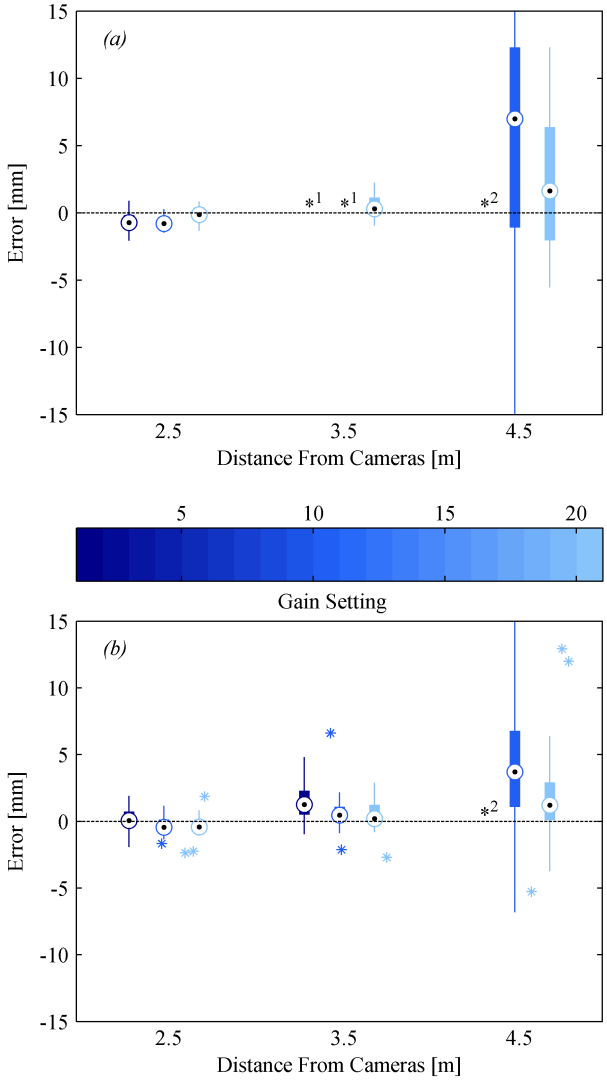

Fig. 8: Absolute measurement errors (e) for each gain setting and camera-target separation. (a) No relative water velocity. (b) Relative water velocity of $\approx$ 2 m/s. Circles denote median values, solid lines denote the 25^{th} to 75^{th} percentile, thin bars denote the extent of measurements beyond the interquartile range, asterisks denote outliers that are beyond 1.5 times the interquartile range. 1: Case not tested. 2: Targets not visible at this gain setting.

due to "trimming" of the black target area by over exposure of the surrounding white space or error in the estimates for camera parameters from the calibration procedure. Although the individual camera pixel error is an order of magnitude smaller than the observed bias, compounding biases from both cameras and two measured positions may approach 2 mm. At a separation of 4.5 m, uncertainties are higher due to the degradation in image quality and can exceed 1 cm. As shown in Fig. 5, images at this distance have little contrast and the precision of corner detection is reduced. Error associated with identifying the same target position in image pairs with low resolution and contrast contribute to greater uncertainty. Measurement errors under test conditions with high relative

TABLE V: Optical imaging capabilities at different target separation distances (visual imagery only in the absence of stereographic or presence/absence information).

Camera-Target Separation Distance	Detection	Discrimination	Classification
2.5 m	Small and large fish	Small and large fish	Small and large fish
3.5 m	Small and large fish	Small and large fish	Large fish only
4.5 m	Large fish only	Large fish only	Unlikely for any fish

water velocity are not markedly different for the 2.5 m and 3.5 m separations. Error decreases for the 4.5 m separation, likely due to decreased frame depth (high wire angle for fixed length umbilical) and increased ambient light levels (at 30 m depth, light levels are estimated to be 5 Lux).

IV. Discussion

The results of laboratory and field evaluations indicate that the optical and acoustic imaging system will be able to perform its desired function for post-installation monitoring of marine animal interactions with tidal turbines. Measurement errors, even at 4.5 m camera-target separation are relatively small, less than 10% of the length of expected small targets (e.g., 10 cm herring). A digital gain setting between $10x$ and $20x$ appears warranted for target detection, discrimination, and classification over a range of camera-target separation distances. The system performs well in high currents, with no obvious degradation in image quality associated with higher levels of flocculent flux. This is ascribed to the camera-light separation distance.

The expected capabilities of the optical imaging system to detect, discriminate, and classify fish targets are summarized in Table V. Detection denotes the ability to locate a target in the camera field of view. Discrimination denotes the ability to distinguish between fish and other targets, such as woody debris or kelp. Classification denotes the ability to achieve a degree of taxonomic grouping. Test data indicates that visual imagery alone is unlikely to be sufficient for species-level classification, but that visual imagery, in addition to stereographic information (e.g., length), and known species presence/absence may be sufficient to achieve this objective. The acoustic camera is capable of detecting targets within the optical camera field of view and will be an effective complement to characterize the behavioral response of fish to strobe illumination.

On this basis, if the intention is to evaluate interactions between marine animals and the turbine rotor, the imaging system should be deployed at turbine hub height at a slant distance of no more than 3-4 m. The capabilities of an imaging system deployed in this manner are shown, conceptually, in Fig. 9 for an OpenHydro turbine.

As a final point of discussion, the volume of data produced by optical imaging systems of this type is daunting, and the use of such a system in an untargeted manner presents the risk of

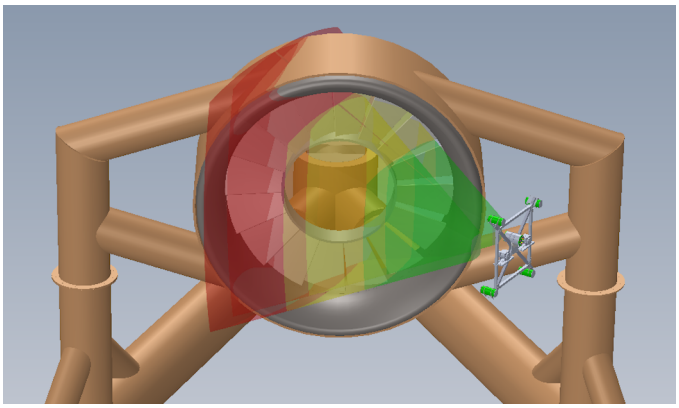

Fig. 9: OpenHydro turbine with camera system FOV. Green prism denotes range at which classification is likely, yellow for discrimination, and red for the extent of possible target detection.

"data poisoning" in which the volume of data produced is too unwieldy to distill and extract information. Highly targeted use to evaluate specific hypotheses is necessary with the system in its current configuration. Potential future enhancements could include automatic image processing routines or real-time, triggered operation (e.g., wide aperture single-beam sonar for automatic target detection and optical camera data for target classification and identification).

V. Conclusion

A hybrid optical-acoustic camera system has been developed to characterize the interactions of marine animals at close range to tidal turbines. Field evaluations conducted under realistic operating conditions indicate that the system will be able to provide useful information to characterize environmental effects that are potentially significant, but subject to high uncertainty.

Acknowledgements

Funding for this project is provided by the US Department of Energy and Snohomish Public Utility District. BlueView provided the acoustic camera under a no-cost lease agreement for evaluation purposes. The authors would also like to thank Jim Thomson for coordination of the field deployments, Sharon Kramer for recommendations on system testing, Capt. Andy Reay-Ellers for captaining the R/V Jack Robertson during the field tests, Alex DeKlerk for designing and fabricating the imaging frame, Joe Talbert and Tim McGinnis for making up the tow umbilical, Nick Stelzenmuller for developing a number of prototype targets, Heather Eberhart for helping with general assembly and cable management, Keith Van Thiel for the design of the pressure housings and optical ports, Rick Towler and Kresimir Williams for insight into component selection and stereographic calibration, and last, but certainly not least, Randy Sindelar for his adaptable, custom electronics for power and communication.

REFERENCES

[1] B. Polagye, B. V. Cleve, A. Copping, and K. Kirkendall, "Environmental effects of tidal energy development," U.S. Dept. Commerce, NOAA Tech. Memo, Tech. Rep. F/SPO-116, 181 p, 2011.

[2] G. Cada, J. Ahlgrimm, M. Bahleda, T. Bigford, S. Stavrakas, D. Hall, R. Moursund, and M. Sale, "Potential impacts on hydrokinetic and wave energy conversion technologies on aquatic environments," *Fisheries*, vol. 32, no. 4, pp. 174–180, 2007.

[3] H. A. Viehman, "Fish in a tidally dynamic region in maine: hydroacoustic assessments in relation to tidal power development," Master's thesis, University of Maine, 2012.

[4] Snohomish PUD, FERC Project No. 12690-000, Final Pilot License Application for the Admiralty Inlet Pilot Tidal Project, 2012.

[5] B. Polagye, M. Kawase, and P. Malte, "In-stream tidal energy potential of Puget Sound, Washington," *Proc. Inst. MechE, Part A: J. Power and Energy*, vol. 223, no. 5, pp. 571–587, 2009.

[6] B. Polagye and J. Thomson, "Tidal energy resource characterization: methodology and field study in Admiralty Inlet, Puget Sound, US," *Proc. IMechE, Part A: J. Power and Energy*, under revision.

[7] H. G. Greene and C. Geology, "Habitat characterization of the snoPUD turbine site - Admiralty Head, Washington State," Final Report, June 2011.

[8] S. Gallager, H. Singh, S. Tiwari, J. Howland, P. Rago, W. Overholtz, R. Taylor, and N. Vine, *Report of the National Marine Fisheries Service Workshop on Underwater Video Analysis*. U.S. Dept. of Commerce, NOAA Tech. Memo., 2005, no. NMFS-F/SPO-68, 69 p, ch. High resolution underwater imaging and image processing for identifying essential fish habitat.

[9] J. S. Jaffe, "Underwater optical imaging: the design of optimal systems," *Oceanography*, pp. 40–41, November 1988.

[10] J. Howland, S. Gallager, H. Singh, A. Girard, L. Abraams, and C. Griner, "Development of a towed survey system for deployment by the fishing industry," *MTS/IEEE Oceans*, 2006.

[11] K. Williams, C. N. Rooper, and R. Towler, "Use of stereo camera systems for assessment of rockfish abundance in untrawlable areas and for recording pollock behavior during midwater trawls," *Fishery Bulletin*, vol. 108, pp. 352–362, 2010.

[12] J. Y. Bouguet. Camera calibration toolbox for Matlab. [Online]. Available: $http://vision.caltech.edu/bouguetj/calib_doc/index.html$

[13] C. Harris and M. Stephens, "A combined corner and edge detector," in *Proceedings of the 4th Alvey Vision Conference*, 1988, pp. 147–151.

[14] G. Xu and Z. Zhang, *Epipolar geometry in stereo, motion, and object recognition: a unified approach*. Norwell, MA: Kluwer Academic Publs., 1996.

[15] J. S. Jaffe, "Multi autonomous underwater vehicle optical imaging for extended performance," in *IEEE Oceans*, San Diego, CA, June 2007.